Separation of unsaturated C18 fatty acids using perfluorinated-micellar electrokinetic chromatography: II) role of nano-structuration

Hai Yen Ta, Christophe Déjugnat, Stéphane Balayssac, Fabrice Collin, Stéphanie Balor, Véronique Gilard, François Couderc

Separation of unsaturated C18 fatty acids using perfluorinated-micellar electrokinetic chromatography: II) Role of nano-structuration

*Hai Yen Ta[a], Christophe Déjugnat[a], Stéphane Balayssac[a], Fabrice Collin[a], Stéphanie Balor[b], Véronique Gilard[a], François Couderc[a,]**

a Laboratoire des IMRCP, Université de Toulouse, CNRS UMR 5623, Université Toulouse III – Paul Sabatier, France

b Plateforme de microscopie électronique intégrative METi, IEFG CNRS IFR 109, Bat. IBCG, 118 route de Narbonne, 31062 Toulouse, France

Corresponding author: Pr François COUDERC, Laboratoire des IMRCP, Université de Toulouse, CNRS UMR 5623, Université Toulouse III - Paul Sabatier. 118 route de Narbonne, 31062 TOULOUSE CEDEX 4 ; France. Tel (+33) (0)561558873. francois.couderc@univ-tlse3.fr

Highlights

- Free fatty acids are separated by capillary electrophoresis using fluorosurfactants
- Scattering experiments evidence aggregation from small micelles to large structures
- Micelle structuration in injection buffer and background electrolytes is affected by fatty acids
- Selective interactions between fatty acids and fluorosurfactant allow CE separation

Abstract

Three fatty acids were separated by micellar electrokinetic chromatography (MEKC) using ammonium perfluorooctanoate as volatile surfactant. Characterizations of both injection buffer and background electrolyte have been performed by complementary techniques including scattering experiments (light, x-rays) and NMR. Different structures have been observed such as small micelles at low methanol content and larger aggregates at high methanol content. In both cases fatty acids interact specifically with the perfluorinated self-assemblies due to different geometrical constraints and different interactions between polar head groups, ensuring separation by MEKC.

Abbreviations: Alpha linolenic acid ALA, Ammonium perfluorooctanoate APFOA, Background electrolyte BGE, Elaidic acid EA, Fatty acids FAs, Linoleic acid LA, Micellar electrokinetic chromatography MEKC, Oleic acid OA, Perfluorooctanoic acid PFOA.

Keywords

Self-assembly, surfactant, MEKC, light scattering, SAXS, NMR, fatty acids

1. Introduction

Capillary electrophoresis (CE) is an analytical technique which allows separation of charged analytes based on their electrophoretic mobilities in an applied electric field. In the case of neutral compounds, additional structured charged fluids are required to achieve separation. The use of charged micelles has been largely developed in Micellar Electro Kinetic Chromatography (MEKC) [1]. Separation is there determined by competitive hydrophobic interactions and equilibrium between aqueous bulk and hydrophobic micellar cores acting as pseudo-stationary phase. Sodium dodecyl sulfate is the most widely used surfactant in MEKC, most of the time associated to cyclodextrins. Although efficient, this surfactant is not volatile and does not allow mass spectrometry (MS) detection in the case of trace amounts. One of the less developed application of CE is the separation of lipids [2]. However, this technique was recently shown to be particularly powerful to separate unsaturated fatty acids using a very simple buffer composed of a buffering salt, Brij 35 as surfactant, and large amount of organic solvent (50%) [3]. Adding sodium dodecylbenzenesulfonate to supplement the latter buffer, the separation of saturated and unsaturated fatty acids was realized using indirect UV detection [4]. Why the use of CE for free fatty acids analysis would be better than the one of the very classical and robust gas chromatography (GC)? Because fatty acids have to be derivatized into fatty acid methyl esters (FAMEs) prior to GC analysis. The preparation of FAMEs is long, because of the extraction/methylation steps and might cause autooxidation of fatty acids when polyunsaturated. Moreover, the CE can be easily applied in routine applications, such as analysis of food supplements in the form of oil, mainly containing triglycerides of fatty acids. In this case, a simple saponification followed by a dilution is enough to prepare the sample before injection. More generally, compared to other separation techniques (*e.g.* HPLC or gel electrophoresis), CE is a very attractive analytical method from the view of environmental and economical aspects. Indeed, this simple and miniaturized techniques requires only very small volumes of analytes and solvents (few µLs per analysis) [5]. In a previous paper, we have shown that SDS/cyclodextrin can be efficiently replaced by ammonium perfluorooctanoate (APFOA), a volatile perfluorinated surfactant, for the separation of a series of fatty acids [6]. It could be mentioned here that perfluorocarboxylates are persistant compounds which have been detected

in various natural environments. Methods have been reported for the removal and recycling of APFOA from waste water, especially membrane nanofiltration [7], which can be envisaged here for the reusability of APFOA after CE analysis and sample collection. We showed that the most unsaturated species were migrating first while the less unsaturated ones were eluted with the highest migration times. We wanted to understand how separation of free fatty acids could be possible in such perfluorinated medium while perhydrogenated/perfluorinated interactions are known to be not favored. Only few studies report the mesostructures of such micellar electrolytes although this is important for understanding how separation proceeds [8,9]. The aim of the present study is thus to characterize the structuration of the complex fluids involved during the separation of fatty acids, namely oleic acid (OA), linoleic acid (LA), and alpha-linolenic acid (ALA) in the presence of APFOA as surfactant (the structures of these compounds are reported in Figure 1). We have used complementary techniques such as scattering experiments (x-rays, light), microscopy, CE, and NMR. We propose a mechanism to rationalize the observed separation.

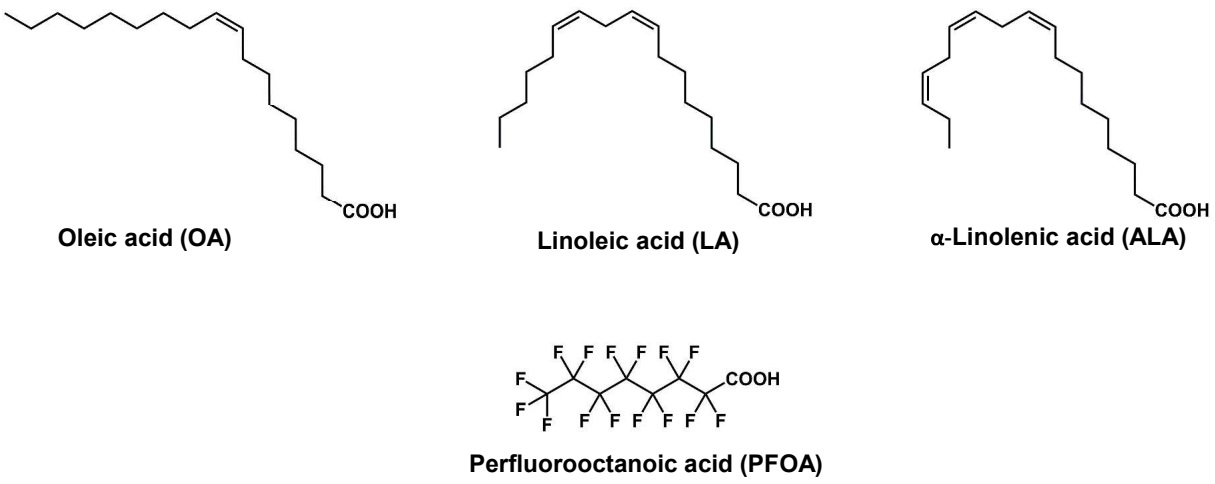

Figure 1. Structures of the studied compounds: fatty acids and perfluorosurfactant

2. Materials and methods

2.1. Materials

Perfluorooctanoic acid (PFOA, 96 %), oleic acid (OA, ≥ 99%), linoleic acid (LA, ≥ 99%), alpha-linolenic acid (ALA, ≥ 99%), 2,2,2-trifluoroethanol (TFE), sodium hydroxide, ammonium hydroxide (25 M in water), methanol (HPLC grade), and water (HPLC grade) were purchased from Sigma-Aldrich (Saint-Quentin-Fallavier, France). Deuterated solvents were supplied from Eurisotop (Saint-Aubin, France).

2.2. Sample preparation

Stock solutions of ammonium perfluorooctanoate (APFOA) were prepared by dissolving the appropriate amount of PFOA in aqueous NH_4OH at a given ratio R = $[NH_4OH]/[PFOA]$. The pHs of these stock solutions were measured using a Seven Compact S220 pH-meter (Mettler Toledo). Stock solutions of FAs (30 mM) were prepared in MeOH and kept at 5 °C before use. The background electrolytes (BGEs) and the injection buffer (INJ) were obtained from the stock solutions of APFOA and FAs, adjusting the target concentrations by addition of water and MeOH.

2.3. Multi-angle light scattering (MALS)

MALS measurements were performed on a 3D LS Spectrometer from LS Instruments (Fribourg, Switzerland) equipped with a 100 mW high performance DPSS Laser (Cobolt, λ = 660 nm), an automated laser attenuation system combined with on-line laser intensity measurement, a two-channel multiple tau correlator (auto and cross correlation, 1088 real time channels), a 3D cross-correlation module, and a variable-angle detection system equipped with two high sensitivity APD detectors. Samples were introduced into cylindrical glass cells (10 mm diameter) that were placed in a sample chamber filled with index-matching fluid (mixed cis-trans decaline); temperature control was ensured by an external circulator (Julabo CF31). Measurements were performed at 25°C for scattering angles θ ranging from 12° to 150°, corresponding to scattering wave vectors $q=[4\pi \cdot n \cdot \sin(\theta/2)]/\lambda$ ranging from 3×10^{-4} $Å^{-1}$ to 2×10^{-3} $Å^{-1}$ (n=1.330 is the refractive index of water). When preliminary measurements indicated multiple scattering, the 3D cross-correlation configuration[10] was required to discard the multiple scattering contribution from the total scattered light. At each angle, 3 to 10 measurements were carried out and averaged. Analysis of dynamic light scattering measurements were performed using the home-made MULTI-STORMS software developed by Dr. C. Mingotaud (see *Supporting Information*), while static light scattering measurements were analyzed using the SasView software (http://www.sasview.org/), version 4.2.2. (M. Doucet et al. SasView Version 4.2.2, Zenodo, http://doi.org/10.5281/zenodo.2652478). Full equations are reported in the *Supporting Information S2-S3*.

2.4. Small-angle x-ray scattering (SAXS)

SAXS measurements were performed on a Xeus 2.0 SAXS beamline for laboratory from Xenocs (FERMAT Federation, Toulouse), equipped with an internal copper source producing 8 keV x-rays (λ = 1.54 Å) and a Pilatus 1 M pixel detector from Dectris. The sample-to-detector distance was 1216.5 mm corresponding to a covered q range from 6×10^{-3} $Å^{-1}$ to 5×10^{-1} $Å^{-1}$. For each sample, 6 scans of 10 min were recorded and averaged. The observed intensities I(q) were corrected for transmission, solvent, and detector response. Absolute intensities I(q) (cm^{-1}) were obtained after standard normalization. As

for static light scattering, analyses of the I(q) profiles were realized using SasView. Full equations are reported in the *Supporting Information*.

2.5. Nuclear magnetic resonance (NMR)

Solutions were prepared using deuterated solvents. NMR experiments were performed on a Bruker Avance 400 spectrometer (Bruker Biospin AG, Fallanden, Switzerland) equipped with a 5 mm triple resonance probe (TXO) at 298 K. All ^{1}H NMR and DOSY experiments were performed on mixtures containing FAs and trifluoroethanol (TFE) as a reference.

Quantitative ^{1}H NMR spectra with pre-saturation pulse for HOD signal suppression were acquired with the following parameters: acquisition time of 2.93 s, 30° pulse, relaxation delay of 12s, for a spectral width of 14 ppm and a number of scans of 64. Under these recording conditions, the ^{1}H resonances were fully relaxed since a repetition time upper than 15 s did not modify the signal intensities.

The DOSY spectra were acquired with the stebpgp1s program from Bruker library pulse sequences. All spectra were recorded with 32K data points, 12 ppm for spectral width, 3 s for relaxation delay and 16 scans. The pulse field gradient length and the diffusion time were optimized for each samples and were 3.6-4.0 s and 160-250 ms respectively. The gradient strength was linearly incremented in 16 steps from 5 % up to 95 % of the maximum gradient strength.

All NMR data were processed using the TOPSPIN 4.0.8 software with one level of zero-filling and an exponential line-broadening function of 0.3 Hz. Spectra were calibrated at 3.88 ppm on the CH_2 NMR signal of TFE. The data sets of diffusion NMR experiments were processed with TOPSPIN software and transferred to the Origin 9.1 software. The exponential fit tool was then used to determine the values of the self-diffusion coefficients (D).

2.6. Capillary electrophoresis (CE)

CE analysis were performed on an Agilent Technologies CE7100 instrument (Waldbronn Germany). Separations of FAs were carried out on a 50 µm id x 365 µm od x 51 cm effective length (59 cm total length) bare-fused silica capillary (Picometrics - Adelis Technologies, Labège, France).

New capillaries were rinsed with 1 M NaOH for 60 min, water (HPLC grade) for 30 min, and background electrolyte (BGE) for 15 min. Between analysis, capillaries were rinsed with methanol for 3 min, 1 M NaOH for 3 min, water for 2 min, and BGE for 3 min. At the end of each day, capillary was rinsed with methanol for 3 min, 1 M NaOH for 15 min, and water for 5 min. Samples were hydrodynamically injected at 50 mbar for 5 s. All analyses were carried out at 25 °C and the wavelength of UV direct detection was set at 195 nm. The samples were prepared in 53 % (v/v) MeOH APFOA 23 mM, to ensure solubilization of FAs.

2.7. Cryo-Transmission electron microscopy (cryo-TEM)

For cryo-TEM analysis, samples were prepared and analyzed at METi, Toulouse. Samples were deposited onto carbon grids and loaded into the thermostatic chamber of a Leica EMGP automatic plunge Freezer, set at 20 °C and 95 % humidity. Excess solution was blotted with a Whatman filter paper, and the grid was immediately flash frozen in liquid ethane, cooled at -183 °C. Sample observations were performed on a Jeol 2100-EX electron microscope operating at 200 kV. Cryo-TEM image acquisitions were performed with a CCD camera US4000 4k×4k (Gatan) equipped with a post-column energy-filter (Gatan GIF Quantum). Images were recorded with a low electron dose (< $10e^-/Å^2$) at a nominal magnification corresponding to a calibrated pixel size of 1.71 Å. Nominal defocus values ranged from 800 nm to 1200 nm.

3. Results and discussion

3.1. Self-organization of APFOA as a function of methanol content leads to various nanostructuring in buffers

In water (0% MeOH), APFOA has been shown to self-assemble into small micelles as already reported [11]. In the present case, CE separations were achieved using an excess of ammonia with respect to PFOA (ratio R = $[NH_4^+]/[PFOA^-]$ = 5.1, pH = 9.9). As ammonium counter-ions can affect APFOA self-assembly [11–13], we first checked this nano-structuration in water keeping R = 5.1. NMR experiments allowed cmc determination by measuring the variation of the chemical shift as a function of the reciprocal of the concentration (see *Supporting Information S5*). The value found in the absence of methanol was cmc = 28.3 ± 0.2 mM, which is in good agreement with the literature [14]. Light scattering experiments were then conducted but gave no relevant signal due to the very low optical contrast of APFOA (refractive index increment dn/dc close to 0) [15], even at [APFOA] = 100 mM. In contrast, SAXS experiments easily afforded APFOA scattering profiles thanks to the electronic contrast provided by fluorine atoms. They confirmed the formation of small ellipsoidal micelles, in good agreement with the reported data (see *Supporting Information S11*) [16]. Therefore, we can assume that high ammonia concentration has no significant impact on APFOA micellization in water.

In order to study to role of MeOH, the next measurements have been conducted on the solutions used for the CE separation, namely the background electrolyte (BGE, 10% MeOH, 50 mM APFOA, R=5.1) and the injection medium (INJ, 53% MeOH, 23 mM APFOA, R=5.1).

At 10 % MeOH (BGE), the cmc decreased to 19 ± 0.9 mM (as already determined by CE and NMR) [6], evidencing the promoting effect of MeOH on micelle formation. This could be related to the preferential solvation of APFOA by MeOH than by water [17], in a similar way as 10 % ethanol promotes

APFOA micellization, as reported recently [18]. Indeed, the localization of alcohol at the micelles reduces the repulsive interactions between charged head groups by decreasing the surface charge density, which leads to a decrease of the cmc. As observed in pure water, the BGE did not produce relevant light scattering. This was not surprising as the refractive index of the solution (1.335) remained very close to the one of water (1.330) and therefore the optical contrast was not enhanced. Nevertheless, SAXS experiments were successfully performed on this sample, evidencing that small ellipsoidal micelles were still there even in the presence of 10% MeOH in the solution (Figure 2A). The structural parameters have been determined and only show a marginal change compared to the micelles in pure water. This was confirmed by CE analysis, which could also be used to determine the micellar volume, the aggregation number, and the degree of counterion dissociation from the global charge of the micelles (see *Supporting Information S6-S7*). This shows that the APFOA initial micellar structure is maintained in the BGE.

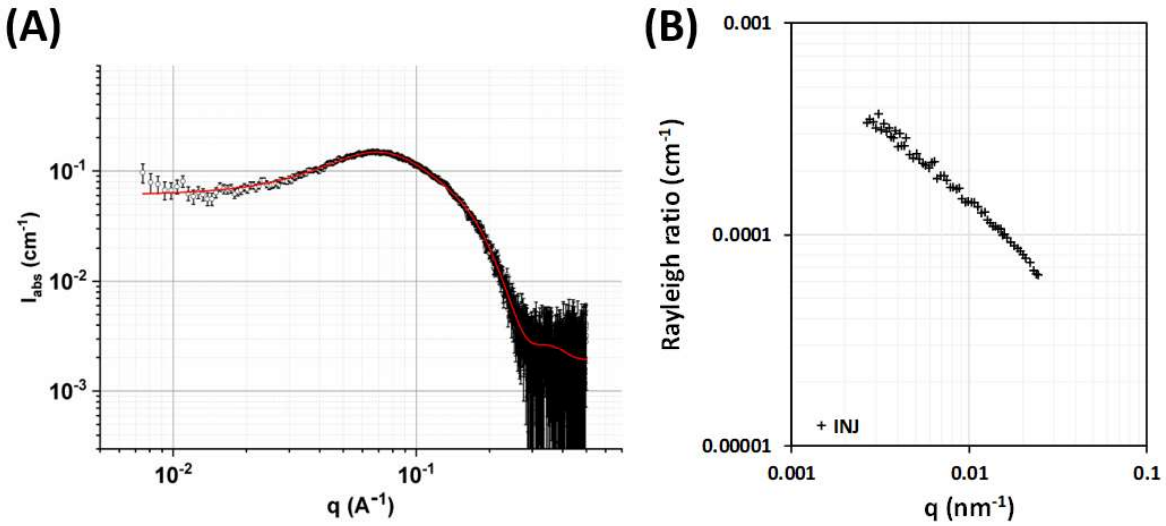

Figure 2. (A, left) SAXS profile of BGE indicating structuration into small ellipsoidal micelles; (B, right) SLS profile of INJ indicating structuration of APFOA into large aggregates

The case of the injection buffer (53% MeOH) was radically different. In SAXS, the signals corresponding to the small micelles completely vanished thus indicating their dissolution. Only an increase of the scattered intensity at very low *q* values could be the sign of the presence of much larger aggregates. Indeed, light scattering was this time much stronger and both DLS and SLS measurements could be accurately performed. As the refractive index of the solution did not increase much (n = 1.341), the increase of light scattering indicated that larger objects were present in the solution. Indeed, the I(q) profile radically changed as illustrated by SLS in Figure 2B. Moreover, both the hydrodynamic radius and the radius of gyration (Rh,Rg = 30-55 nm) observed by CE analysis could not correspond to small micelles (*Supporting Information S7*).

We can conclude that increasing the MeOH content induced a phase transition from small micelles (in BGE) to much larger aggregates (in INJ).

In INJ, the local concentration of MeOH in the solvation sphere of APFOA is close to 75% [17]. We observe a transition from small micelles to larger objects when the amount of alcohol increases. This could be explained first by the local reduction of the dielectric constant which induces a lowering of electrostatic repulsions and therefore a decrease of the interface curvature, like observed in the presence of large counterions or when the ionic strength is high. Moreover, MeOH could also interact with polar heads by forming H-bonds resulting again in a flatter interface by bridging effect [19].

This first set of scattering experiments show that APFOA can self-assemble into different sizes of aggregates, depending on the amount of MeOH. From the CE point of view, the injection buffer initially contains large objects that converted into small ellipsoid micelles upon dilution in the background electrolyte.

3.2. Structuration of the complex fluids (BGE, INJ) in the presence of fatty acids

Here we investigated the impact of dissolved FAs on the microstructures of both BGE and INJ.

Introducing 1mM FA in the BGE did not produced more relevant DLS signal than what observed in pure BGE, while SAXS shows the presence of small micelles nearly identical to APFOA alone (Figure 3A). Although CE separation is the sign that FAs interact with APFOA micelles, the insignificant structural changes observed here could be due to the large ratio between the surfactant and the analytes: [APFOA]/[FA]=50, corresponding to about one FA molecule per APFOA micelle. This could also be due to the dynamic character of micelles with fast exchange between molecules. Nevertheless, this observation indicates that aggregation into small dynamic micelles still occurs in the presence of FA, allowing CE separation**.**

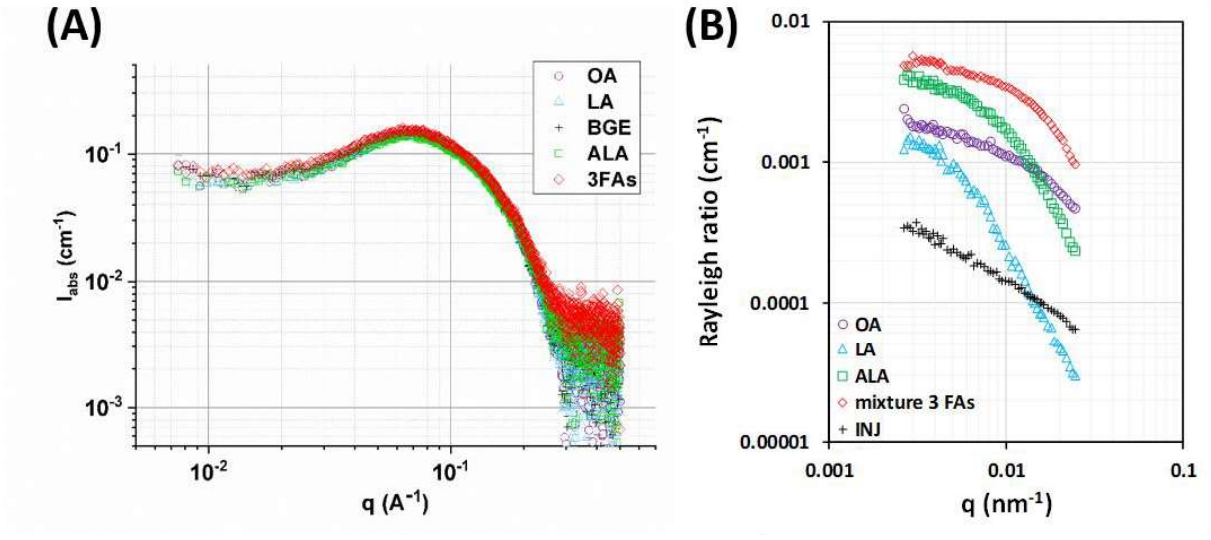

232

233 **Figure 3**. (A, left) SAXS profile of BGE containing FAs indicating structuration into small ellipsoidal
234 micelles; (B, right) SLS profile of INJ indicating structuration of APFOA into large aggregates whose
235 nature depends on FAs.

236 The structuration into small micelles could be detected by cryo-TEM observations as illustrated in
237 Figure 4 in the case of 3mM OA in BGE.

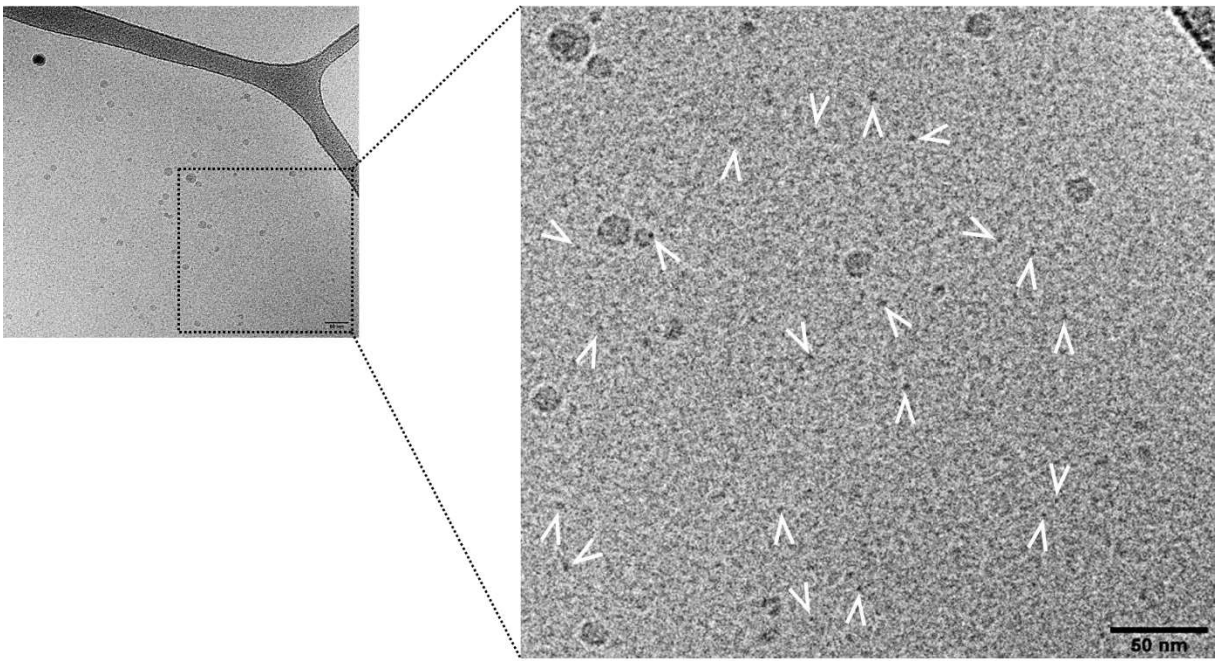

238

239 **Figure 4.** Cryo-TEM micrographs of BGE containing OA (3 mM) and illustrating the structuration into
240 small micelles mainly.

241

At 23 mM APFOA, 53% MeOH (INJ), DLS and SLS measurements evidenced the presence of large aggregates (as observed without FAs), as illustrated for SLS in Figure 3B (DLS are reported in the *Supporting Information*).

SLS profiles show that the presence of FAs impacts the structure of these large aggregates even if the relative amount of FA compared to APFOA remains very low. This is the sign that FAs are present in these large aggregates confirming that hydrogenated FAs can be incorporated in fluorinated APFOA structures. Moreover, the influence of the FA depends on its nature. Large aggregates are only weakly modified by OA; this minor perturbation due to OA incorporation in APFOA aggregates could be related to a matrix effect [20]. Major structural modifications are observed with other FAs probably due to geometric constraints (repulsive interactions): this induced size/shape transitions to structures where FAs (LA, ALA) could be less embedded than OA. The number of unsaturations is responsible for FA different structural geometries: the molecules are bended, in the order OA > LA > ALA (Figure 1), and could explain the easier incorporation of OA in APFOA structures as compared to LA and ALA.

This set of experiments indicates a selective interaction between FAs and APFOA.

3.3. Structuration in the absence of APFOA micelles

We have seen that small APFOA micelles are required to allow CE separation. Here we investigated the behavior of FAs in the absence of APFOA micelles.

First, we replaced APFOA by 50 mM TFA (which cannot form micelles) in the BGE. Unprotonated FAs (soaps) are known to self-assemble in water in various structures depending on pH. At high pH (pH>pKa) small micelles are formed with low cmcs (0.1-0.5 mM) [21–23]. At pH close to pKa, rodlike micelles are formed and they transit to vesicle if pH is further decreased [24]. In the present case, the pH is just above the pKas of FAs which are supposed to potentially self-assemble into micelles. Indeed, DLS showed that FAs formed small spherical micelles (ALA and LA), or elongated ones (OA, pH close to pKa). When mixing the three FAs an average micellization was observed (see *Supporting Information S11*). This evidences that FAs still form dynamic micelles at 10% MeOH, but that the rapid exchange between FA micelles could not allow CE separation in the absence of APFOA micelles. To ensure CE separation, the presence of micelles is required but not sufficient: a selective interaction between FAs and APFOA is needed.

In order to further characterize this selective interaction, we conducted complementary experiments in an intermediate situation where APFOA is present but not in a micellar form (c=10 mM < cmc). In these conditions, CE separation could not be achieved. DLS and SLS measurements showed the formation of large structures (Rh=43 nm, Rg=75 nm) which could not correspond to small micelles

(see *Supporting Information S12*). Additional NMR experiment showed that FAs in the mixed FAs-APFOA aggregates have not the same line width for the NMR signals above or below the cmc of APFOA. A difference in dynamics for these aggregates can explain this observation. Figure 5 presents the comparative ^{1}H NMR signals of terminal CH_3 for each FA at various APFOA concentration.

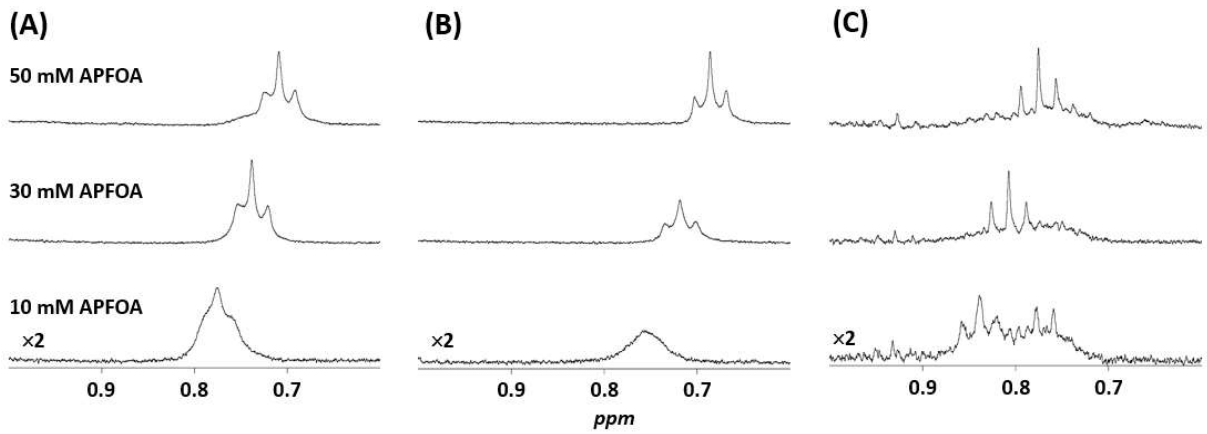

Figure 5. NMR signal of CH_3 (0.6-1.0 ppm) for (A) OA, (B) LA, and (C) ALA at 10, 30, and 50 mM APFOA, respectively.

Below APFOA cmc, the NMR signals for the 3 FAs present large line broadenings: 15.3 Hz, 17.8 Hz, and 4.8 Hz for the CH_3 of OA, LA, and ALA respectively; this indicates that molecules do not diffuse freely and are embedded in weakly dynamic aggregates that do not ensure CE separation. On the contrary, higher dynamics are observed for the CH_3 above the cmc of APFOA (50 mM) with smaller line broadenings at 3.4 Hz, 2.4 Hz, and 1.5 Hz respectively, closer to what observed for free FAs in 100 % MeOD (1.2-1.5 Hz). Moreover, considering the right situation for CE separation (APFOA at 50mM > cmc), we see that the integration of the NMR signals of FA, recorded under the same conditions, are not the same. They increase in the order ALA < LA < OA and the integration ratios OA/ALA and LA/ALA are 2.2 and 1.25 respectively. This observation shows a favored solubilization of OA (followed by LA and ALA), indicating a selective incorporation of FAs in APFOA micelles. This was confirmed by DOSY experiments, giving access to the diffusion coefficients (D) of FAs as a function of APFOA concentration. First in 100% MeOD, the diffusion coefficients of FAs are in the range D = 10.4-11.1 10^{-10} m^2/s. Considering the viscosities of methanol/water mixtures at 25°C reported in the literature (η=1.16 cP for MeOH:H_2O = 10/90 and η=0.54 cP for MeOH:H_2O = 100/0) [25], the diffusion coefficients of free FAs in situation of CE separation were estimated to be about D = 4.6 ± 0.2 10^{-10} m^2/s. However, in mixed FA-APFOA aggregates at 50 mM of APFOA, experimental D are measured at 0.8 ± 0.1, 1.5 ± 0.1 and 2.6 ± 0.1 10^{-10} m^2/s for OA, LA, and ALA, respectively. NMR has evidenced slow diffusion

coefficients for FAs in the order OA<LA<ALA. This again evidences a selective interaction between FAs and APFOA aggregates. This controls the ease of FA incorporation in APFOA micelles as well as the residence time (longer for OA than for LA than for ALA).

3.4. Selective interactions between FAs and APFOA

The selective association between FAs and APFOA result from the contribution of different interactions.

First, at the level of polar head groups, interactions depend on the charge and therefore on the pKa value. It has been reported for FAs that when the pH is close to the pKa (this is here the case for OA, pKa_{OA}=9.85 [26]) then the molecules are only partially charged and interact at the interface in a close way via ion-dipole interactions (Figure 6A) [26–28]. On the other hand, when pH is higher than pKa (case of LA and ALA with pKa_{LA}=9.24 and pKa_{ALA}=8.28 [26]), ionic repulsions between charged polar head groups tend to increase the distance between the molecules at the interface. This might support the fact that OA interacts with APFOA micelles in a more favored way than LA and ALA.

Then at the level of fatty chains (in the micelle core) the hydrophobic interactions depend also on the distance between the tails. From geometric considerations it is clear that it will be impacted by the geometries of FAs, which depend on the number of unsaturations in the chain. Therefore, the steric hindrance will increase in the order OA < LA < ALA and, together with the differences in polar interactions, it will control the differential association of FAs with APFOA micelles (Figure 6B). This general analysis could be extended to other structurally related analytes such as saturated FAs. For such compounds, both higher pKa values and lower steric hindrance (compared to unsaturated FAs) would result in more favorable interactions with APFOA micelles: in that case, we expect a longer elution time. The situation could be more complex for other analytes for which interactions with APFOA might compete in opposite ways. It could be the case for shorter FAs with lower pKas (unfavorable interactions) and reduced steric hindrance (favorable interactions): in that case, the resulting balance of interactions could be difficult to predict.

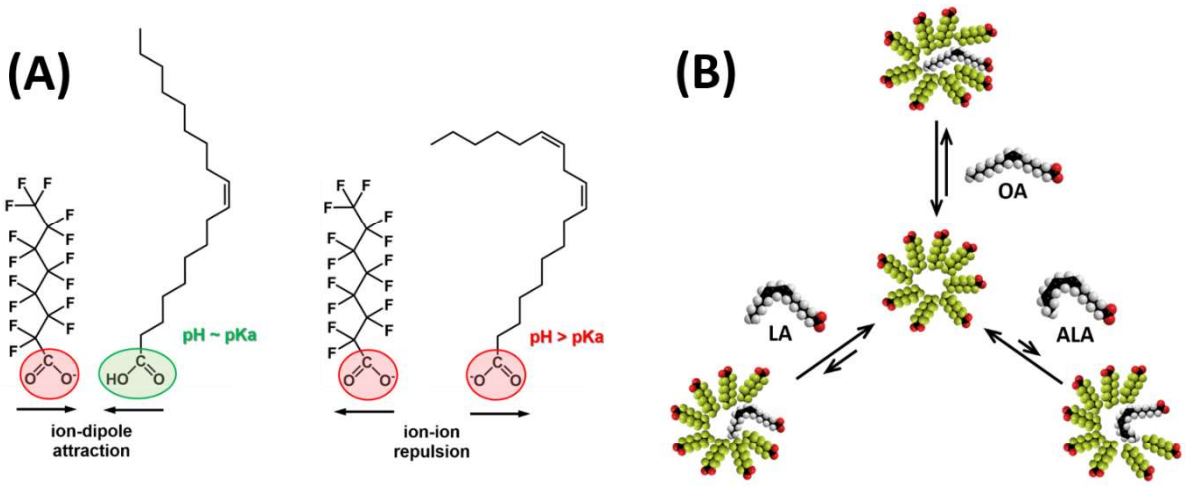

Figure 6. Differential interactions between polar heads and fatty chains that control the overall preferential incorporation of FAs in APFOA micelles. (A) left: when pH is close to pKa, half of FAs molecules are in neutral form and can interact with APFOA by attractive ion-dipole interactions; right: when pH is higher than pKa only ion-ion repulsions occur between charged anionic species. (B) representative scheme illustrating the increasing difficulty of incorporating FAs in APFOA micelles as the molecules become bender and bender in the series OA < LA < ALA (based on geometrical considerations).

Conclusion

Meso-scale characterizations of electrolytes used in CE separation of FAs by APFOA have evidenced the presence of structured complex fluids both in the injection medium (INJ) and in the background electrolyte (BGE). The structuration has been characterized by complementary techniques such as scattering experiments (light, x-rays) and NMR. It has been shown to depend on the amount of MeOH and on the concentration of the surfactant APFOA. First, in INJ (53% MeOH), large aggregates were formed with structures depending on the nature of the incorporated FA, revealing selective interactions between the perfluoosurfactant and the perhydrogenated analytes. Then in BGE (10% MeOH, [APFOA]>cmc), small APFOA micelles were observed which ensured CE separation of FAs. In both cases selective interactions have been related to a subtle interplay between pH, MeOH amount, and APFOA concentration. Considering both chemical and structural parameters of the analytes (pKa, shape), we could propose a global depiction of these systems allowing to rationalize the observed separation. This shows that using micellar systems in MEKC could lead to more complex structures than expected and that structural characterization of the separating fluids could be a prerequisite to understand and potentially anticipate the analytic separation. This work could now be extended not only to the analysis of other important FAs or analytes, but also especially to the use of mass

spectrometry (MS) as detection mode thanks to the volatility of APFOA allowing downscaling of analysis to trace levels.

Acknowledgments

We thank FERMaT, Université de Toulouse, France – CPER IMATECBIO for providing access to the Xeuss 2.0 SAXS instrument (Xenocs), and gratefully acknowledge Dr. Pierre Roblin, (IR, CNRS) IMFT, Toulouse for technical support in SAXS measurements. This work benefited from the use of the SasView application, originally developed under NSF Award DMR-0520547. SasView also contains code developed with funding from the EU Horizon 2020 program under the SINE2020 project Grant No 654000.

References

[1] S.K.D. Alagar Raja M, Bhargav KS, Banji D, Updated Review on Micellar Electro kinetic Chromatography, J. Chromatogr. Sep. Tech. 05 (2014). https://doi.org/10.4172/2157-7064.1000231.

[2] V. Poinsot, H.Y. Ta, V.O. Meang, L. Perquis, P. Gavard, B. Pipy, F. Couderc, A digest of capillary electrophoretic methods applied to lipid analyzes, Electrophoresis. 40 (2019) 190–211. https://doi.org/10.1002/elps.201800264.

[3] T.L. Amorim, L.M. Duarte, M.A. de la Fuente, M.A.L. de Oliveira, P. Gómez-Cortés, Fast capillary electrophoresis method for determination of docosahexaenoic and eicosapentaenoic acids in marine oils omega-3 supplements, J. Chromatogr. A. 1613 (2020) 460641. https://doi.org/10.1016/j.chroma.2019.460641.

[4] T.L. Amorim, M.G.D.R. Pena, F.F. Costa, M.A.L. de Oliveira, P.R. Chellini, A fast and validated capillary zone electrophoresis method for the determination of selected fatty acids applied to food and cosmetic purposes, Anal. Methods. 11 (2019) 5607–5612. https://doi.org/10.1039/C9AY01917K.

[5] Z. Gao, W. Zhong, Recent (2018–2020) development in capillary electrophoresis, Anal. Bioanal. Chem. 414 (2022) 115–130. https://doi.org/10.1007/s00216-021-03290-y.

[6] H.Y. Ta, L. Perquis, S. Balayssac, C. Déjugnat, A. Wodrinski, F. Collin, V. Gilard, F. Couderc, Separation of unsaturated C18 fatty acids using perfluorinated-micellar electrokinetic chromatography: I) Optimization and separation mechanism study, Submitted. (2022).

[7] X. Hang, X. Chen, J. Luo, W. Cao, Y. Wan, Removal and recovery of perfluorooctanoate from

wastewater by nanofiltration, Sep. Purif. Technol. 145 (2015) 120–129. https://doi.org/10.1016/j.seppur.2015.03.013.

[8] P.G. Muijselaar, H.A. Claessens, C.A. Cramers, Evaluation and characterization of pseudo-stationary phases in micellar electrokinetic chromatography, Chromatographia. 45 (1997) 433–434. https://doi.org/10.1007/BF02505596.

[9] C. Fu, M.G. Khaledi, Characterization and Classification of Pseudo-Stationary Phases in Micellar Electrokinetic Chromatography Using Chemometric Methods, Anal. Chem. 86 (2014) 2371–2379. https://doi.org/10.1021/ac403231h.

[10] I.D. Block, F. Scheffold, Modulated 3D cross-correlation light scattering : Improving turbid sample characterization, Rev. Sci. Instrum. 81 (2010) 123107. https://doi.org/10.1063/1.3518961.

[11] C. Zhang, L. Yang, K. Zhao, Z. Chen, J.-X. Xiao, Effect of counterions on anionic fluorocarbon surfactant micelles by dielectric spectroscopy, New J. Chem. 42 (2018) 14210–14218. https://doi.org/10.1039/C8NJ02524J.

[12] O. Regev, M.S. Leaver, R. Zhou, S. Puntambekar, Counterion Effects on Aggregate Size and Shape in Dilute Binary Solutions of Fluorinated Ammonium Carboxylate Surfactants, Langmuir. 17 (2001) 5141–5149. https://doi.org/10.1021/la001232e.

[13] C. Wang, P. Yan, H. Xing, C. Jin, J.-X. Xiao, Thermodynamics of Aggregation of Ammonium/Tetraalkylammonium Perfluorooctanoates: Effect of Counterions †, J. Chem. Eng. Data. 55 (2010) 1994–1999. https://doi.org/10.1021/je900916e.

[14] H. Xing, S.-S. Lin, R.-C. Lu, J.-X. Xiao, NMR investigation on micellization of ammonium/tetraalkylammonium perfluorooctanoates, Colloids Surfaces A Physicochem. Eng. Asp. 318 (2008) 199–205. https://doi.org/10.1016/j.colsurfa.2007.12.033.

[15] G. Pößnecker, H. Hoffman, The Refractive Index of Perfluorinated Surfactant Solutions, Berichte Der Bunsengesellschaft Für Phys. Chemie. 94 (1990) 579–583. https://doi.org/10.1002/bbpc.19900940509.

[16] M.J. Pottage, T.L. Greaves, C.J. Garvey, R.F. Tabor, The effects of alkylammonium counterions on the aggregation of fluorinated surfactants and surfactant ionic liquids, J. Colloid Interface Sci. 475 (2016) 72–81. https://doi.org/10.1016/j.jcis.2016.04.039.

[17] S. Kutsuna, H. Hori, T. Sonoda, T. Iwakami, A. Wakisaka, Preferential solvation of perfluorooctanoic acid (PFOA) by methanol in methanol–water mixtures: A potential

overestimation of the dissociation constant of PFOA using a Yasuda–Shedlovsky plot, Atmos. Environ. 49 (2012) 411–414. https://doi.org/10.1016/j.atmosenv.2011.12.009.

[18] D. Dong, S. Kancharla, J. Hooper, M. Tsianou, D. Bedrov, P. Alexandridis, Controlling the self-assembly of perfluorinated surfactants in aqueous environments, Phys. Chem. Chem. Phys. 23 (2021) 10029–10039. https://doi.org/10.1039/D1CP00049G.

[19] C.L. Apel, D.W. Deamer, M.N. Mautner, Self-assembled vesicles of monocarboxylic acids and alcohols: conditions for stability and for the encapsulation of biopolymers, Biochim. Biophys. Acta - Biomembr. 1559 (2002) 1–9. https://doi.org/10.1016/S0005-2736(01)00400-X.

[20] S. Rasi, F. Mavelli, P.L. Luisi, Matrix Effect in Oleate Micelles-Vesicles Transformation, Orig. Life Evol. Biosph. 34 (2004) 215–224. https://doi.org/10.1023/B:ORIG.0000009841.20997.ac.

[21] K. Theander, R.J. Pugh, The Influence of pH and Temperature on the Equilibrium and Dynamic Surface Tension of Aqueous Solutions of Sodium Oleate, J. Colloid Interface Sci. 239 (2001) 209–216. https://doi.org/10.1006/jcis.2000.7543.

[22] N. El Kadi, F. Martins, D. Clausse, P.C. Schulz, Critical micelle concentrations of aqueous hexadecytrimethylammonium bromide-sodium oleate mixtures, Colloid Polym. Sci. 281 (2003) 353–362. https://doi.org/10.1007/s00396-002-0783-z.

[23] J. Verhagen, J.F.G. Vliegenthart, J. Boldingh, Micelle and acid-soap formation of linoleic acid and 13-L-hydroperoxylinoleic acid being substrates of lipoxygenase-1, Chem. Phys. Lipids. 22 (1978) 255–259. https://doi.org/10.1016/0009-3084(78)90014-2.

[24] K. Suga, D. Kondo, Y. Otsuka, Y. Okamoto, H. Umakoshi, Characterization of Aqueous Oleic Acid/Oleate Dispersions by Fluorescent Probes and Raman Spectroscopy, Langmuir. 32 (2016) 7606–7612. https://doi.org/10.1021/acs.langmuir.6b02257.

[25] S.Z. Mikhail, W.R. Kimel, Densities and Viscosities of Methanol-Water Mixtures., J. Chem. Eng. Data. 6 (1961) 533–537. https://doi.org/10.1021/je60011a015.

[26] J.R. Kanicky, D.O. Shah, Effect of degree, type, and position of unsaturation on the pKa of long-chain fatty acids., J. Colloid Interface Sci. 256 (2002) 201–7. https://doi.org/10.1006/jcis.2001.8009.

[27] J.R. Kanicky, A.F. Poniatowski, N.R. Mehta, D.O. Shah, Cooperativity among Molecules at Interfaces in Relation to Various Technological Processes: Effect of Chain Length on the p K a of Fatty Acid Salt Solutions †, Langmuir. 16 (2000) 172–177. https://doi.org/10.1021/la990719o.

452 [28] J.R. Kanicky, D.O. Shah, Effect of Premicellar Aggregation on the p K a of Fatty Acid Soap
453 Solutions, Langmuir. 19 (2003) 2034–2038. https://doi.org/10.1021/la020672y.

454